Assessment of Dynamic Range and Noise in a Natural-Scene Image

Seungwan Jeon, En-Ji Young, DongOh Kim, DongYoung Song, KiChul Park, Sung-Su Kim, and Yitae Kim; S.LSI Division, Samsung Electronics; Hwaseong-si, Gyeonggi-do, Republic of Korea

Abstract

In photography, the dynamic range (DR) is a distinguishable brightness range and is determined by the analog-to-digital converter (ADC) and signal-to-noise (SNR) performance of the sensor. Recently, many various HDR strategies have been introduced to obtain high DR beyond these hardware limitations. However, since camera manufacturers set these HDR algorithms to operate differently by considering the situation, it is necessary to evaluate the quality of images taken in various situations for objective evaluation. In order to quantitatively measure the DR, we should know both the actual luminous intensity and the SNR of the picture. However, it is difficult to measure the two information in general-scene photos without charts. To overcome these problems, in this study, we propose a method to measure the DR of a natural-scene photograph by reconstructing radiance map and specifying the pixel value at which the SNR reaches 12dB. Using the pre-calculated radiation and SNR information, we measured DR of photos without using a chart, and demonstrated that HDR images have higher DR than standard DR (SDR) images.

Introduction

In photography, dynamic range (DR) is defined as a ratio between the lowest and highest brightness where the signals are distinguishable. One of the primary factors that determines the DR of a camera sensor is an analog-to-digital converter (ADC). Nowadays, 10-bit ADCs are most commonly used in mainstream mobile cameras, and theoretically, those can have about 60-dB DR. Another factor that limits the DR is noise. Noise as strong as a signal makes it difficult to distinguish the signals, resulting in a reduction of DR. To overcome these hardware limitations, many camera manufacturers try to adopt various high DR (HDR) reconstruction strategies that synthesize multiple images with modulated shutter speed or gain. To measure the DR, it is required to find the minimum/maximum brightness, which is distinguished in a picture. Conventionally, the actual brightness is measured via illuminant DR chart. Through the known luminance ratios of the DR chart, we can acquire a function representing the relationship between the actual radiance and the recorded pixel value, which is called as a camera response function (CRF). Referring to the definition of DR as the maximum/minimum brightness ratio in which signals are distinguished, DR is determined as a radiance section in which the CRF slope and the SNR are maintained above a certain level. Normally, the criteria of the CRF slope is defined as 7.5% of its maximum slope and that of the SNR is defined as 0, 6, 12, or 20dB [1].

However, there is a limitation in the DR measurement of today's mobile phones. In order to optimize the quality of the merged HDR images, camera manufacturers perform quite complex HDR algorithms while considering the internal and external conditions of the camera in combination. Thus, depending on the situation, the DR performance could not be constant, and it may be limited by unexpected side effects. In addition, the DR performance of sensors is usually measured in a laboratory environment with well-controlled light conditions, whereas practical environments have various light conditions. Because of the difference, the specification of the DR measured in a laboratory could be differ from the real user experience. For this reason, there have been demands to measure the DR in various situations to evaluate it in a multifaceted and objective manner. However, it has been a challenging problem to measure image quality, such as SNR, without relying on reference charts.

To solve this problem, in this study, we propose a method to measure the DR and SNR of a natural-scene (NS) photo. To overcome the lack of radiance reference, we reconstructed a pseudo radiance reference map by adopting Devec's HDR recovery method [2]. Further, we improved the robustness of its CRF estimation method by correcting a defect caused by scale mismatch in the optimization equation. For specifying the pixel value satisfying the SNR-based criteria of DR measurement, we developed a method which can measure SNR according to pixel values. This proposed method can assess the noise even in images with few flat areas, such as a NS image, by locally calculating the averages (AVG) and the standard deviations (STD) via an adaptive anisotropic kernel. Through the radiation and SNR according to pixel levels, we could quantify the DR of NS images by determining the distinguishable brightness where the contrast and SNR were maintained above a certain level. Then, we verified the methods we developed through simulation and actual tests and confirmed the consistency with qualitative evaluation.

Methods

Modified CRF

In order to find distinguishable brightness, the CRF must be obtained first. Although DR chart is conventionally used for this, we used the HDR radiation map (HDR-RM) introduced in the Devec's paper [2] as our pseudo radiation reference to measure DR in NS images without the chart. The first step to recover the HDR-RM is to estimate CRF by using multiple standard DR (SDR) images with various exposure times (multi-EIT SDR images). According to Devec, et al., the log-scaled inverse CRF, g, can be derived as follows:

$$z_{ij} = f\left(E_i \Delta T_j\right), \tag{1}$$

$$log_{10} f^{-1}\left(z_{ij}\right) = log_{10} E_i + log_{10} \Delta T_j, \tag{2}$$

$$g\left(z_{ij}\right) = log_{10} E_i + log_{10} \Delta T_j, \tag{3}$$

where z_{ij} is the i-th pixel value at j-th shutter speed, E_i is the irradiance at the i-th pixel, ΔT_j is j-th shutter speed, and f is the CRF.

From the above equations, the inverse CRF can be estimated by optimizing the following equation:

$$\underset{g(z),E}{\mathrm{argmin}} \left[\sum_i \sum_j [w(z_{i,j})(g(z_{i,j}) - log_{10} E_i - log_{10} \Delta T_j)]^2 + \lambda \sum_z \left[w(z) \frac{d^2 g(z)}{dz^2} \right]^2 \right], \tag{4}$$

where $w(z)$ is a triangular weighting function that is maximized at the half of the maximum pixel level, λ is a regularization coefficient (0.1 used in this paper). In the equation (4), the regularization term, including the Laplacian of g, is added to make the curve smooth, but the $g(z)$ is the exposure of logarithmic scale whereas z is the pixel value of linear scale. This disparity makes the CRF estimation unstable. To solve this problem, we modified the equation so that both scales can be unified. From the equations (1-3),

$$z_{ij} + 1 = f(E_i \Delta T_j) + 1, \tag{5}$$

$$log_2(z_{ij} + 1) = log_2(f(E_i \Delta T_j) + 1)$$

$$= \hat{f}(E_i \Delta T_j), \tag{6}$$

$$log_{10} \hat{f}^{-1}(log_2(z_{ij} + 1)) = log_{10} E_i + log_{10} \Delta T_j, \tag{7}$$

$$\hat{g}(log_2(z_{ij} + 1)) = log_{10} E_i + log_{10} \Delta T_j. \tag{8}$$

Accordingly, the loss function in equation (4) was modified as

$$\underset{\hat{g}(log_2(z_{i,j}+1)),E}{\mathrm{argmin}} \left[\sum_i \sum_j [w(z_{i,j})(\hat{g}(log_2(z_{i,j} + 1)) - log_{10} E_i - log_{10} \Delta T_j)]^2 + \lambda \sum_{log_2(z_{i,j}+1)} \left[w(z_{ij}) \frac{d^2 \hat{g}(log_2(z_{i,j}+1))}{d\,log_2(z_{i,j}+1)^2} \right]^2 \right]. \tag{9}$$

Note that the modified inverse CRF function, $\hat{g}$, receives the log-scaled pixel value. Thus, the regularization term could converge to zero when the pixel value linearly increases with exposure.

CRF of a Test Image

To acquire the CRF of a test image, we need the following steps: 1) generate a reference radiance map; 2) extract sample pairs from both the radiance map and the test image; and 3) define the CRF through regression (Figure 1). For the reference radiance map, we followed the same method in the Devec's research, recovering the HDR-RM by blending the multi-EIT SDR images converted to radiation values through the obtained inverse CRF as follows:

$$log_{10} E_i = \frac{\sum_{j=0}^{P-1}[w(z_{ij})(\hat{g}(log_2(z_{ij}+1)) - log_{10} \Delta T_j)]}{\sum_{j=0}^{P-1} w(z_{ij})}. \tag{10}$$

In the sampling process, we extracted radiance-pixel level samples pairs considering the distribution of the radiance, so that the regression can be conducted stably as follows:

$$S_{Radiance} = \{r_{x,y}|(x,y) \in S\}, \tag{11}$$

$$S_{pixel\ level} = \{i_{x,y}|(x,y) \in S\}, \tag{12}$$

where $S = \{(x,y)|\phi < m \cdot \chi_{x,y}, \phi \sim U[0,1]\}$ denotes radiance-uniform random sampling map as, m is the desired number of samples to extract, $\chi_{x,y} = \frac{h_R(\lfloor \frac{r_{x,y}}{\Delta b} \rfloor)}{\sum_{x,y} h_R(\lfloor \frac{r_{x,y}}{\Delta b} \rfloor)}$, is the probability density map for the radiance uniformity, $h_R(n)$ is the histogram of the radiance map with the interval of Δb, and $(r_{x,y}, i_{x,y})$ are the values of the HDR-radiance map and the test image at (x,y).

Then, we obtained the CRF of a test image, $f_{radiance}: Radiance \rightarrow PixelValue$, by conducting locally weighted scatterplot smoothing (LOWESS) method.
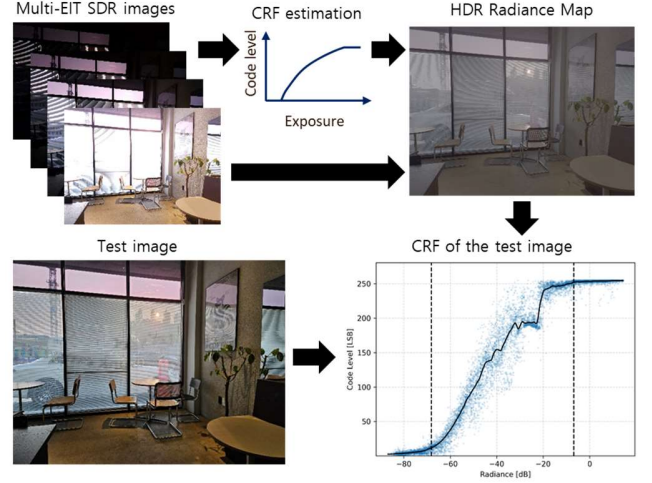
Figure 1. Process to recover HDR-RM and to acquire the CRF of a test image. The dashed lines in CRF of the test image represent the determined min/max DR cutoff, which is described later.

Determination of CRF Slope

Due to variations in image signal processing (ISP) strategies, such as tone mapping, among phone manufacturers, the CRF may operate irregularly at times. So, we proposed a method of measuring the slope that is robust to the scale of uncertain pixel levels and unpredictable its fluctuations. For the scale robustness, we calculated correlations between the log-scaled pixel level and the radiance and between the linear-scaled and the radiance. Then, determined one with high correlation as the real scale (Figure 2ab). Based on the selected scale, we fitted a curve, f_{fitted}, as below to the radiance-pixel level samples, and used 7.5% of the slope of the curve, $0.075a$, as the slope-based DR cutoff criteria (Figure 2c):

$$f_{fitted} = min(max(ax + b, Z_{max}), Z_{min}). \tag{13}$$
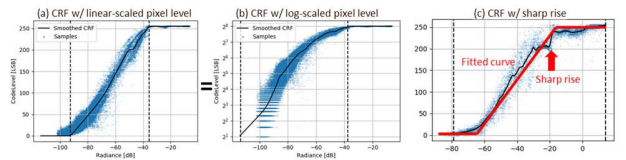
Figure 2. (a-b) An example of CRF with linear- or log-scaled pixel level, (c) an example with sharp rise and its fitted curve.

Local Average & Standard Deviation Maps

For SNR measurement, we calculated the average (AVG) and sample standard deviation (STD) locally with an anisotropic kernel in a direction consistent with that of the edge which can be represented as:

$$\mu_{x,y,\theta_{optimal}} = I_{x,y} * k(\theta_{optimal}), \tag{14}$$

$$\sigma_{x,y,\theta_{optimal}} = \sigma_{x,y}(\theta_{optimal}), \tag{15}$$

where

$$k(\theta) = \frac{1}{2\pi\sqrt{|\Sigma|}} e^{-0.5(X^T\Sigma^{-1}X)}, \tag{16}$$

$$\Sigma = RSSR^{-1}, \ R = \begin{bmatrix} \cos\theta & -\sin\theta \\ \sin\theta & \cos\theta \end{bmatrix}, \ S = \begin{bmatrix} \lambda_1 & 0 \\ 0 & \lambda_2 \end{bmatrix}, \tag{17}$$

$$\theta_{optimal} = \underset{\theta}{argmin}\, \sigma_{x,y}(\theta), \tag{18}$$

$$\sigma_{x,y}(\theta) = \sqrt{\left(I_{x,y} - I_{x,y} * k(\theta)\right)^2 * \frac{\lambda_1\lambda_2}{\lambda_1\lambda_2-1} k(\theta)}. \tag{19}$$

$I_{x,y}$ is the original image, $k(\theta)$ is a multivariate 2D Gaussian kernel rotated by θ and the sum of each element is 1, and (λ_1, λ_2) are the eigenvalues of the covariance matrix of the $k(\theta)$ (7 and 1 were used respectively, in this study). Note that, in the equation (19), is a mean subtraction and contrast normalization (MSCN) equation [3] in which only the kernel is replaced from a normal Gaussian to the multivariated 2D Gaussian, and $\frac{\lambda_1\lambda_2}{\lambda_1\lambda_2-1}$ is a factor to correct the error caused by sample standard deviation assuming that the area of the kernel is equal to $\lambda_1\lambda_2$.
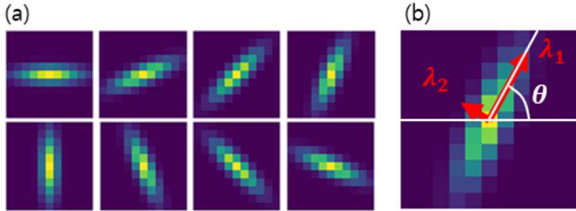
Figure 3. (a) multivariate 2D Gaussian kernels with various directions, (b) proposed kernel according to the eigenvalues and the direction of the covariance matrix.

SNR Function of a Test Image

To acquire the function of SNR according to the pixel level, we extracted the 20,000 AVG & STD value pairs considering both the AVG uniformity and the flatness as belows:

$$S_{AVG} = \left\{\mu_{x,y,\theta_{optimal}} | (x,y) \in S\right\}, \tag{20}$$

$$S_{STD} = \left\{\sigma_{x,y,\theta_{optimal}} | (x,y) \in S\right\}, \tag{21}$$

where

$$S = \left\{(x,y) | \phi < n \cdot \frac{\psi_{x,y}\rho_{x,y}}{\Sigma(\psi_{x,y}\rho_{x,y})}, \phi \sim U[0,1]\right\}, \tag{22}$$

$\psi_{x,y}$ is a probability density map for AVG uniformity which can be acquired in the same way of that of the radiance uniformity, $\rho_{x,y}$ is a probability density map for flatness. Inspired by Frangi filter [4], we calculated the $\rho_{x,y}$ as follows:

$$\rho_{x,y} = e^{-\left(\frac{\sqrt{\hat{\lambda}_{1,x,y}^2 + \hat{\lambda}_{2,x,y}^2}}{2\tau_{40\%}}\right)^2} \tag{23}$$

where $(\hat{\lambda}_{1,x,y}, \hat{\lambda}_{2,x,y})$ are the eigenvalues of Hessian matrix of the test image, and $\tau_{40\%}$ is the threshold that satisfies $P\left(\sqrt{\hat{\lambda}_{1,x,y}^2 + \hat{\lambda}_{2,x,y}^2} < \tau_{40\%}\right) = 40\%$. Note that $\rho_{x,y}$ has high weight on the bottom 40% with low eigenvalues, which means that the value is likely to be extracted if its position is flat regardless of horizontal or tilted. Then we conducted the LOWESS regression on the AVG & STD sample pairs to obtain the STD function, f_{STD}: AVG → STD. Although the STD samples are the sample STD, the expected STD of the STD function converges to population STD due to the averaging effect in this regression process. Sequentially, we could simply get the SNR function as $f_{SNR} = 20\log\frac{AVG}{f_{STD}(AVG)}$.

Through the CRF and SNR functions, we found both slope- and SNR-based DR cutoffs. The maximum DR cutoff was acuiqred as follows:

$$C_{max} = max\{r | 0.075a < \nabla f_{radiance}(r)\}. \tag{24}$$

where r is the log-scaled radiance and a is the CRF slope in the equation (13). Meanwhile, the minimum DR cutoff was determined based on both criteria as follows:

$$C_{min} = max \begin{pmatrix} min\{r | 0.075a < \nabla f_{radiance}(r)\}, \\ min\left\{r | 12db \le f_{SNR}\left(f_{radiance}^{-1}(r)\right)\right\} \end{pmatrix} \tag{25}$$

Finally, we calculated the DR as follows:

$$DR = C_{max} - C_{min}. \tag{26}$$

Results

Simulation test

We compared the CRFs of 10-bit uncompressed image data estimated by the conventional and proposed CRF estimation methods with the same input data and regularization term (Figure 4). In the result, we confirmed that the CRF inferred by the existing method was not properly optimized, whereas that inferred by the proposed method showed significantly improved optimization stability.
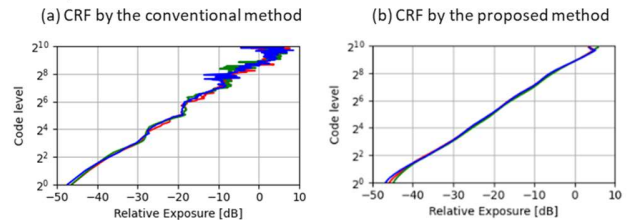
Figure 4. Comparison of CRFs estimated by (a) conventional and (b) proposed methods. CRF, camera response function.

In order to verify the slope-based DR measurement, we simulated multi-EIT 10-bit images to recover the HDR-RM and generated test images with various bit depths by using an open-source HDR image data [5]. Theoretically, DR increases by 6 dB as the bit depth increases by 1 bit. In the results, the DRs were measured to be 60, 71, 81, and 94 dB in the 10-/12-/14-/16-bit images, respectively, which is close to the theoretical expectation.
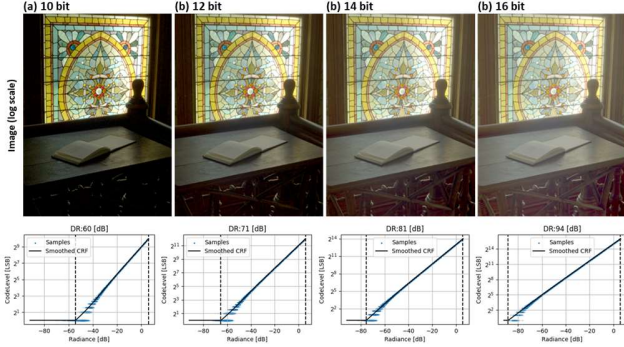
Figure 5. Simulated image with various bit depth and the DR measured by our proposed slope-based DR measurement method.

We also simulated grid- and star-patterned images with Gaussian noise to evaluate our proposed SNR measurement method. We measured the SNRs of the images and compared them with the reference SNR, $f_{SNR,Ref}(x) = 20 \log \frac{x}{\sigma}$, where x is the pixel level and σ is the added Gaussian noise. In both grid-/star-patterned images, we observed that the measured SNR values were well matched with the reference above 10 dB, even though the star-patterned image lacks a horizontal and flat area. However, the SNRs were found to be larger than the reference values below 10 dB.
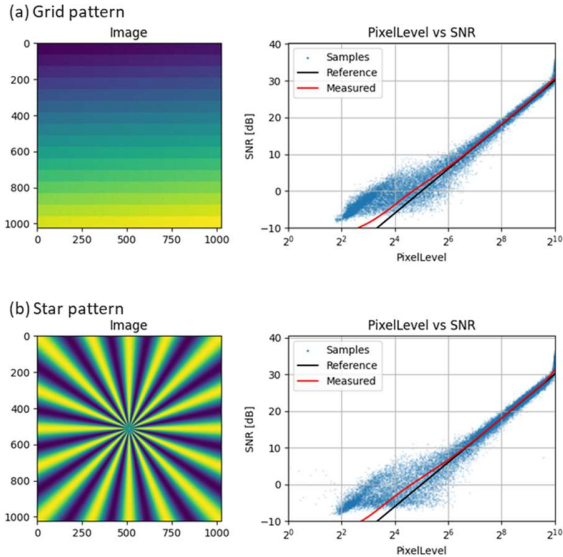
Figure 6. Simulation images and pixel level-to-SNR graphs of (a) grid pattern and (b) star pattern.

To check if our proposed method can properly represent the DR reduction effect due to SNR deterioration, we measured the SNR and DR of images with various noises added to a 16-bit simulation image. As the noise was increased by 4 times, we confirmed that the pixel level to reach 12-dB SNR was also increased by 3.5 and 4.1 times. Accordingly, the minimum DR cutoff increased, lowering DR by 10, 12 dB.
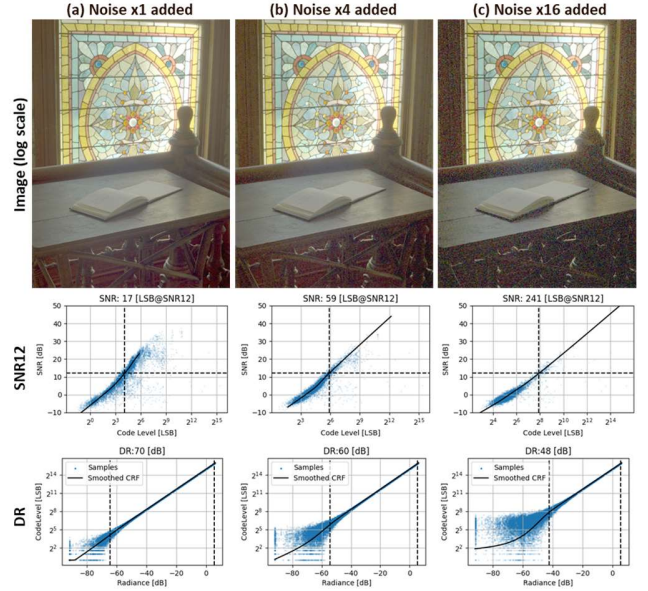
Figure 7. Simulated 16-bit images with various noise level, measured pixel level to reach 12-dB SNR, and measured DR considering SNR.

Actual test

We also compared SDR and HDR images qualitatively and quantitatively (Figure 8). The SDR and HDR images were captured by a mobile phone with HDR-off and HDR-on mode, respectively. In the SDR image, it was difficult to identify some regions due to the saturated signal in the bright area. On the other hand, the HDR image showed better contrast than the SDR image in the corresponding regions. Apart from brighter regions, the HDR image exhibited better quality in dark areas, allowing us to identify more objects than in the SDR image. In the SNR measurement result, SDR and HDR images achieved 12-dB SNR at the pixel values of 13.7 and 6.08, respectively. In the DR measurement result, HDR image showed significantly wider DR than SDR image by 33 dB.
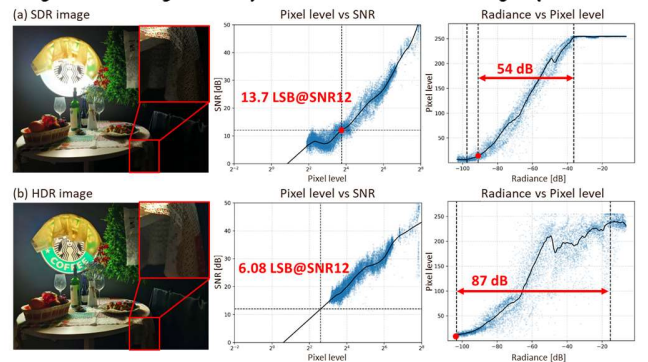
Figure 8. *SNR and DR comparison of SDR and HDR images.*

Discussion

In the SNR measurement process, we proposed a sampling method so that lots of samples could be extracted in flat areas regardless of whether it is tilted or not. This works in harmony with the orientation optimization effect of the adaptive anisotropic kernel, so that the directions of the tile and the kernel are set to be perpendicular to each other. These properties effectively can minimize errors of the SNR calculations. Therefore, this strategy helps to calculate SNR in NS images without charts.

In the simulation test for SNR with grid-/star-patterned image, the measured SNR were mismatched with the reference. However, this is due to the unsigned image data clipping the negative signals to zero, overestimating the SNR values as follows:

$$\frac{\mu}{\sigma} = SNR_{NoClipped} < SNR_{Clipped} = \frac{\mu + \varepsilon}{\sigma - \epsilon}$$

where (μ, σ) are the original average and standard deviation, respectively, and (ε, ϵ) are increase and decrease by the clipping effect. Statistically, only 0.003% signals are clipped when $\mu = 4\sigma$, which is 12 dB. That is why we set the 12-dB SNR as the DR criteria. In the experimental results, it can be seen that there is little error above about 10 dB.

In our study, we employed a kernel with a fixed aspect ratio of 7:1, simplifying the kernel's area as the product of its eigenvalues. However, the optimal kernel characteristics may vary based on the size of the images or the features of the objects under consideration. Thus, our further study includes the exploration of adaptive kernel aspect ratios, considering the diverse nature of images and objects, Additionally, a comprehensive theoretical investigation into determining optimal kernel area for various scenes should be also conducted. Our another further study is to correct the motion error in the CRF estimation as well as HDR-RM generation. Instead of utilizing conventional charts, we adopted the HDR-RM derived from multi-EIT SDR images as the reference for radiance measurement. However, capturing the data in the presence of dynamic object in NS image is practically constrained due to the motion. Consequently, we aim to minimize the motion errors by employing techniques such as optical flow [6] during the data acquisition process.

Conclusion

In this study, we enhanced the optimization accuracy by modifying the existing radiation estimation method. Additionally, we developed a method capable of estimating SNR even in images with few flat areas, employing adaptive anisotropic kernels. Finally, we integrated these two methods to measure DR in photographs, even in scenarios without charts, demonstrating substantial numerical differences between SDR and HDR photos. Therefore, the proposed method is anticipated to offer objective indicators in diverse environments by eliminating environmental restrictions on the measurement of camera SNR and DR performance

References

[1] Imatest, "Dynamic Range," Imatest, [Online]. Available: https://www.imatest.com/solutions/dynamic-range/. [Accessed 30 1 2024].

[2] P. E. a. J. M. Debevec, "Recovering high dynamic range radiance maps from photographs," in *Seminal Graphics Papers: Pushing the Boundaries*, 1997.

[3] A. A. K. M. a. A. C. B. Mittal, "No-reference image quality assessment in the spatial domain," in *IEEE Transactions on image processing 21.12*, 2012.

[4] A. F. N. W. J. V. K. L. &. V. M. A. Frangi, "Multiscale vessel enhancement filtering," in *Medical Image Computing and Computer-Assisted Intervention—MICCAI'98: First International Conference Cambridge, MA, USA, October 11–13*, 1998.

[5] G. Ward, "High Dynamic Range Image Examples," Anyhere Software, [Online]. Available: http://www.anyhere.com/gward/hdrenc/pages/originals.html. [Accessed 1 2 2024].

[6] H. A. B. a. J. W. Zimmer, "Freehand HDR imaging of moving scenes with simultaneous resolution enhancement," %1 *Computer Graphics Forum. Vol. 30. No. 2. Oxford, UK: Blackwell Publishing Ltd*, 2011.

Author Biography

Seungwan Jeon was born in Republic of Korea in 1989. He received the B.S. degree in biomedical engineering from Yonsei University in 2014, and the Ph.D. degree in creative IT engineering from POSTECH in 2020. His Ph.D. research focused on photoacoustic/ultrasound imaging techniques using image/signal processing, beamforming, and deep learning. Since 2020, he is with Samsung Electronics, Republic of Korea, as a Staff engineer. His current research interests include camera sensor, computer vision, and image quality assessment.